

Wigner crystallization at graphene edges

A. D. Güçlü¹

¹*Department of Physics, Izmir Institute of Technology, IZTECH, TR35430, Izmir, Turkey*

(Dated: October 21, 2015)

Using many-body configuration interaction techniques we show that Wigner crystallization occurs at the zigzag edges of graphene at surprisingly high electronic densities up to 0.8 nm^{-1} . In contrast with one-dimensional electron gas, the flat-band structure of the edge states makes the system interaction dominated, facilitating the electronic localization. The resulting Wigner crystal manifests itself in pair-correlation functions, and evolves smoothly as the edge electron density is lowered. We also show that the crystallization affects the magnetization of the edges. While the edges are fully polarized when the system is charge neutral (i.e. high density), above the critical density, the spin-spin correlations between neighboring electrons go through a smooth transition from antiferromagnetic to magnetic coupling as the electronic density is lowered.

Wigner crystallization, i.e. localization of electrons induced by electron-electron interactions¹, remains a key issue in strongly interacting systems. In an electron gas, as the electronic density is reduced, the Coulomb repulsion energy overcomes the kinetic energy and the electrons become localized at their classical positions. The two limits, high density Fermi liquid and low density Wigner crystal, are well understood. However, the crossover in between is a complex many-body problem which was previously investigated for various electron gas systems in various dimensions both theoretically²⁻¹³ and experimentally¹⁴⁻¹⁹. In particular, it is expected that Wigner crystallization has important implications on transport properties of two-dimensional¹⁴ and one-dimensional^{9,12,16-19} systems.

For graphene²⁰⁻²³, the investigation of Wigner crystallization remains limited²⁴⁻²⁷ partially due to the fact that for massless Dirac electrons with linear dispersion (as opposed to quadratic dispersion of free electron gas), the interaction strength does not depend on electronic density²⁸. It is however possible to induce a mass term, for instance, through application of external magnetic field, for which the Wigner crystal regime was studied within meanfield theory^{24,25}, or through size quantization²⁷. Another situation where Wigner crystallization in graphene may occur is when zigzag edges are present as suggested in Ref.26. However, as far as we know, there is no detailed analysis of the many-body problem of Wigner crystal transition at graphene edges. Indeed, zigzag edges give rise to a band of half-filled degenerate states near the Fermi level without the need for an external magnetic field. Electrons populating these edge states constitute a particularly interesting many-body system since their relative kinetic energy is close to zero, thus the properties are dominated by Coulomb interactions. So far, most of the previous literature on interaction effects due to edge states in various graphene systems focused on magnetic properties²⁸⁻⁴¹. In particular, room-temperature magnetic properties of zigzag edge state in graphene nanoribbons were recently investigated experimentally⁴². However, for the design of carbon-based next-generation devices such as nanoribbons²⁹⁻³⁶

and quantum dots³⁷⁻⁴¹, an in-depth understanding of Wigner crystallization at graphene edges is necessary and a focused investigation of the liquid to crystal crossover is lacking.

In this work, we use a combination of tight-binding method and configuration interaction technique on a two-dimensional honeycomb lattice to show that strong Wigner crystallization does indeed occur at zigzag edges as the electronic density is varied. An analysis of the pair-correlation functions shows that the critical electronic density where the localization occur is close to 0.8 nm^{-1} , a value much higher than the critical density for a one-dimensional (1D) electron gas. Indeed, for the 1D electron gas the formation of a Wigner crystal was observed using tunneling spectroscopy into a quantum wire and clear evidence of electron localization was found at a density of $\rho^{1D} \sim 20 \text{ } \mu\text{m}^{-1}$ ¹⁵ whereas Quantum Monte Carlo calculations give $\rho^{1D} \sim 15 \text{ } \mu\text{m}^{-1}$ ¹², both significantly lower than the critical density at the graphene edges found in this work. Finally, we investigate ground state magnetization and spin-spin correlations functions between neighboring electrons to show that the spin correlations are strongly tied to the formation of 1D Wigner crystal as a function of electronic density.

In order to model the interaction effects at the zigzag edges, we start with a graphene ribbon with periodic boundary condition³⁶, consisting of $N_a = 1456$ atoms, with a length of $L = 12.8 \text{ nm}$ and a width of $W = 2.9 \text{ nm}$. This gives $n_s = 15$ edge states on each edge, which are computed using tight-binding technique within next nearest neighbour approximation of p_z orbitals. The nearest-neighbour and next-nearest-neighbour hopping elements are taken to be $t_{nn} = -2.8 \text{ eV}$ and $t_{nnn} = -0.1 \text{ eV}$ ²¹. In addition, since our main goal is to investigate the Wigner crystal properties of a single edge, a small electric-field perturbation perpendicular to the edges was added in order to decouple the states belonging to opposite edges. Next, the fifteen edge states belonging to the upper edge (see Fig.1) were used to compute two-body scattering matrix elements $\langle ps|V|df \rangle$ in terms of the two-body localized p_z orbital scattering matrix elements $\langle ij|V|kl \rangle$. Slater type orbitals⁴¹ were used to calculate

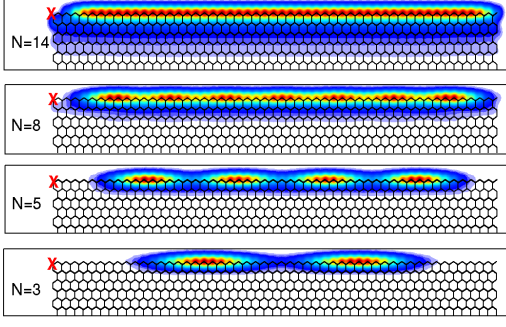


FIG. 1: Two-dimensional pair-correlation functions for $N=14$, 8, 5, and 3 electrons occupying the zigzag graphene edge. The position of the fixed electron is indicated by a cross (red online). At $N=14$ charge oscillations only at the atomic level are observed. At lower N values, $N-1$ peaks arise and become increasingly localized, indicating the formation of an one-dimensional Wigner crystal.

the scattering matrix elements. As the overlap between the bulk state wavefunctions and the edge state wavefunctions is small, electronic correlations between them is expected to be weak and the configuration interaction calculations can be performed in the subspace of edge states³⁶. Finally, ground states in subspaces (N, S_z) with different electron number N occupying the edge states and z -component of the total spin S_z are found using diagonalization of the many-body Hamiltonian given by

$$H_{MB} = \sum_{s,\sigma} E_s a_{s\sigma}^\dagger a_{s\sigma} + \frac{1}{2} \sum_{\substack{s,p,d,f, \\ \sigma,\sigma'}} \langle sp | V | df \rangle a_{s\sigma}^\dagger a_{p\sigma'}^\dagger a_{d\sigma'} a_{f\sigma}. \quad (1)$$

Here, E_s are the kinetic energies in the nearly degenerate shell of edge states. By comparing the ground state energies of different (N, S_z) subspaces, it is then possible to deduce the ground state total spin S . In this work, the dimension of the largest matrix we have diagonalized using Lanczos technique is 2927925×2927925 .

In systems with, e.g. translational or rotational symmetry, electronic localization can be conveniently investigated through pair-correlation functions:

$$P_{\sigma_1\sigma_2}(\mathbf{r}_1, \mathbf{r}_2) = \langle n_{\sigma_1}(\mathbf{r}_1) n_{\sigma_2}(\mathbf{r}_2) \rangle = \sum_{\sigma_3, \dots, \sigma_N} \int d\mathbf{r}_3 \dots d\mathbf{r}_N \times |\Psi(\mathbf{r}_1, \sigma_1; \dots; \mathbf{r}_N, \sigma_N)|^2 \quad (2)$$

which gives the conditional probability to find an electron with spin σ_1 at the position \mathbf{r}_1 provided another electron with spin σ_2 is located at \mathbf{r}_2 . Figure 1 shows the pair-correlation functions for different electron numbers N populating the edge states. The fixed electron

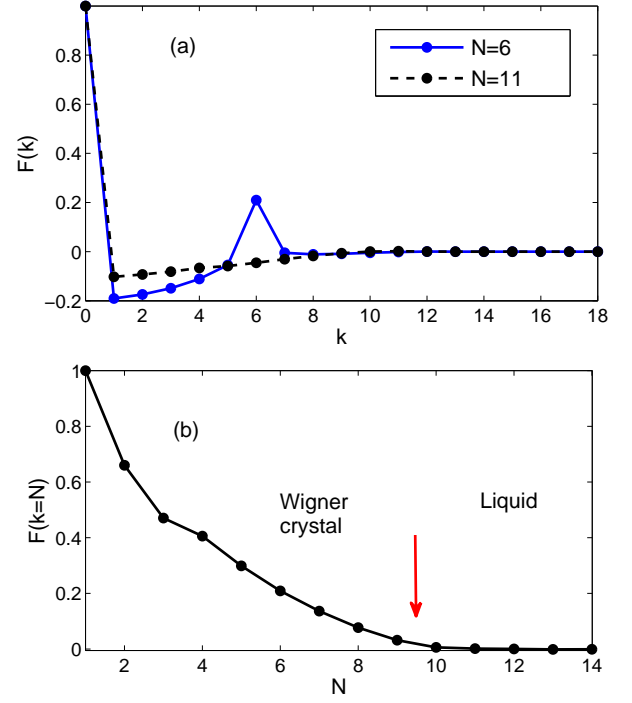


FIG. 2: (a) Power spectrum as a function of Fourier component k for $N=6$ electrons (solid lines, blue online) and $N=11$ electrons (dashed lines). For $N=6$, a peak at $k=6$ is observed which is an indication of charge localization at classical locations. (b) Power spectrum peak height at $k=N$ as a function of N . Above $N=10$, the peak height is practically zero which indicates a lack of Wigner crystallization. The solid-liquid crossover occurs at a one-dimensional density of 0.8 nm^{-1} .

has spin up and is located at the position indicated by a cross. At $N=14$, i.e. close to charge neutrality, no charge inhomogeneities (except due to localization over single atoms) is observed. However, when the density is reduced oscillations start to appear. At $N=8$, oscillations are weak but seven peaks (not counting the fixed electron) are observed which is an indication of Wigner crystallization. At lower densities, localization is strongly enhanced and the overlap between the electrons is close to zero.

Although the pair-correlation plots are convenient for visualization of Wigner crystallization, they do not allow to quantify the degree of localization and to pinpoint the liquid to crystal crossover. This can be achieved by analyzing the power spectrum⁸, i.e. the Fourier transform $F(k)$ of $P_{\sigma\sigma_0}(\mathbf{r}, \mathbf{r}_0)$ in the x direction along the ribbon. In Fig. 2a, we show $F(k)$ for six and eleven electrons. For six electrons, we clearly see a peak at $k=6$, a signature of electronic localization at their classical positions⁸. For $N=11$ however, no localization is observed, indicating that the electronic density is too high to allow for Wigner crystallization. In order to pinpoint the electronic den-

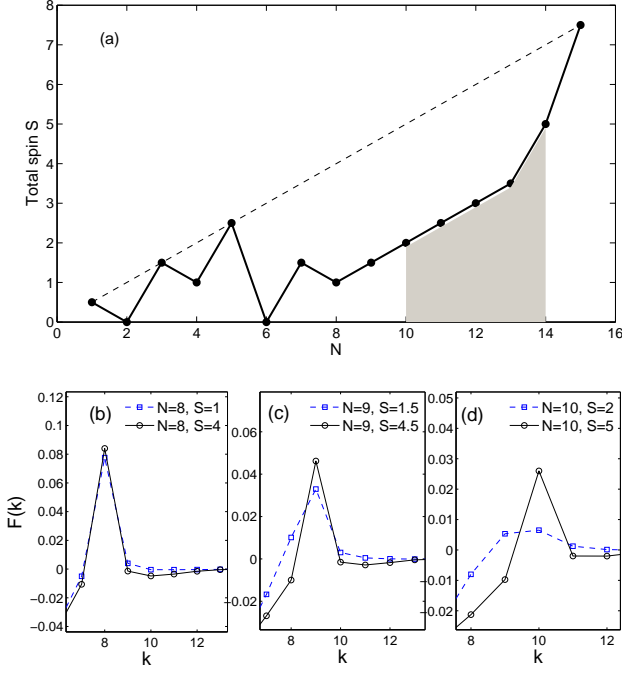


FIG. 3: (a) Ground state total spin S as a function of number of edge electrons N . Dashed line shows the maximum possible total spin and the shaded area indicates the uncertainty in the total spin due to computational limitations. At $N = 15$ the system is charge neutral and the edges are fully polarized. Away from charge neutrality a reduction in magnetization occurs. (b)-(d) Spin dependence of the power spectra for $N = 8, 9$, and 10 .

sity where the localization occurs, Fig.2b shows the power spectrum peak height $F(k = N)$ for N up to fourteen. We see that, as the electronic density is decreased, the peak height decreases, indicating a transition toward liquid state. Above $N = 10$, no localization is observed. In particular, the system is in a liquid state in the vicinity of charge neutrality, i.e. $N = 15$. The crossover value corresponds to a one-dimensional density of 0.8 nm^{-1} . This value is strikingly higher than the critical density for 1D electron gas for which experimental observations¹⁵ and theoretical calculations¹² give $n^{1D} \sim 15 - 20 \mu\text{m}^{-1}$.

We now analyze the ground state magnetic properties as a function of electronic density. Figure 3a shows the ground state total spin S as a function of number of edge electrons N . It is well established that, in agreement with Lieb's theorem⁴³, charge neutral system give rise to ferromagnetic edges. In our case, this means that for $N = 15$, the total spin is $S_{max} = 15/2$. However, away from charge neutrality, correlation effects are expected to strongly affect the magnetization³⁶. In Fig.3a, the dashed line shows the maximum possible polarization. The shaded area indicates an uncertainty in S due to computational limitations, since it becomes exponentially more difficult to diagonalize matrices for small values of S_z at large N . Thus, the solid line in this area

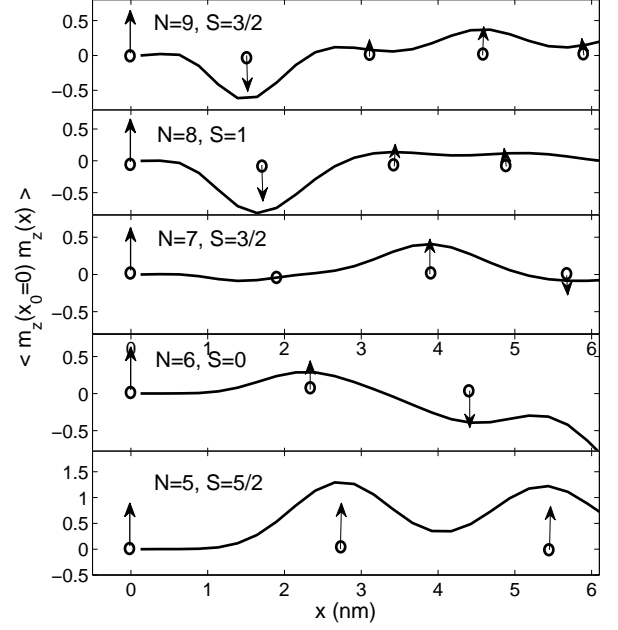


FIG. 4: Ground state spin-spin correlation function along the graphene edge for $N = 9, 8, 7, 6$, and 5 . The small circles with arrows represent the classical position of the localized electrons and their effective spin relative to the fixed electron at $x = 0$. As the density is lowered, the magnetic correlation between the nearest neighbors switches from antiferromagnetic coupling to ferromagnetic coupling. The vertical scale is kept the same in all the panels.

represents an upper limit to S . However, the uncertainty does not affect our estimation of the critical density of Wigner crystallization since the crystallization is already very weak at these N values. Nevertheless, a clear reduction in magnetization, which is consistent with but more pronounced than in previous calculations for smaller system sizes³², is observed. In Fig.3b-d, we also investigate the spin dependence of the power spectra for $N = 8, 9$, and 10 . For the fully polarized state, $S = N/2$, the power spectrum peak height is found to be always higher than the depolarized ground state, indicating stronger localization. However, the difference becomes negligible below $N = 9$ which is another indication that the system enters the Wigner crystal regime⁸.

In order to investigate further the connection between the Wigner crystallization and the ground magnetization, in Fig.4 we plot the ground state spin-spin correlation functions $\langle m_z(x_0)m_z(x) \rangle$ along the edge atoms, where $m_z = n_\uparrow - n_\downarrow$. The small circles with arrows represent the classical position of the localized electrons and their effective spin relative to the fixed electron at $x = 0$. For $N = 9$, Wigner localization has already started but it is weak, with a ground state total spin of $S = 3/2$. The spin-spin correlation function at the nearest neighbors is negative, indicating antiferromagnetic coupling.

For $N = 8$, the spin-spin correlation function does not change significantly compared to the $N = 9$ case. However, as the electronic density is decreased further, the average distance between the electrons increases faster, and the magnetic correlations are affected accordingly. As a result, for $N = 7$ and $S = 3/2$, the magnetic correlations between the nearest electrons drops significantly, and become ferromagnetic for $N = 6$ and $S = 0$. This ferromagnetic coupling between the nearest electrons is further enhanced for $N = 5$ and $S = 5/2$. These results show that the magnetization of the edges is closely tied to the evolution of the Wigner crystallization.

To conclude, we have shown that a one-dimensional Wigner crystallization occurs at the zigzag edges of graphene. An analysis of pair-correlation functions through configuration interaction calculations indicates that the crossover from the Fermi liquid to Wigner solid occurs near a strikingly high critical density of 0.8 nm^{-1} , as compared to the critical density $n^{1D} \sim 15 - 20 \mu\text{m}^{-1}$ for the one-dimensional electron gas. While the spin of the ground state of the charge neutral system is fully polarized, we observe magnetic depolarization and oscillations as the liquid-solid crossover occurs. By analyzing the spin-spin correlations between the neighboring elec-

trons, we have shown that the magnetic oscillations are accompanied by a transition from antiferromagnetic to ferromagnetic coupling between the localized electrons. Localization effects can be observed for instance using tunneling spectroscopy measurements as was done for a one-dimensional electron gas¹⁷. Clearly, for the design of carbon-based spintronic devices, Wigner crystallization must be taken into account for the full understanding of charge and spin transports. Finally, we note that although we have considered an ideal edge without any structural imperfections, inhomogeneities are expected to amplify and not wash out the liquid to crystal transition⁶. Thus, in more realistic graphene structures Wigner crystallization should be even more robust, strongly affecting both the transport and spin properties. Identification of combined effects of imperfections and interaction induced localization requires further investigations.

Acknowledgment. This work was supported by The Scientific and Technological Research Council of Turkey (TUBITAK) under the 1001 Grant Project Number 114F331 and by Bilim Akademisi - The Science Academy, Turkey under the BAGEP program. The author thanks Pawel Hawrylak, Harold U. Baranger and Nejat Bulut for valuable discussions.

-
- ¹ E. Wigner, Phys. Rev. 46, 1002 (1934).
 - ² B. Tanatar and D. M. Ceperley, Phys. Rev. B **39**, 5005 (1989).
 - ³ A. V. Filinov, M. Bonitz, and Yu. E. Lozovik, Phys. Rev. Lett. **86**, 3851 (2001)
 - ⁴ C. Attaccalite, S. Moroni, P. Gori-Giorgi, and G. B. Bachelet, Phys. Rev. Lett. **88**, 256601 (2002).
 - ⁵ X. Waintal, Phys. Rev. B **73**, 075417 (2006).
 - ⁶ A. Ghosal, A. D. Güçlü, C. J. Umrigar, D. Ullmo, and H. U. Baranger, Nature Phys. **2**, 336 (2006)
 - ⁷ A. Ghosal, A. D. Güçlü, C. J. Umrigar, D. Ullmo, and H. U. Baranger, Phys. Rev. B **76**, 085341 (2007)
 - ⁸ A. D. Güçlü, A. Ghosal, C. J. Umrigar, and H. U. Baranger, Phys. Rev. B **77**, 041301(R) (2008).
 - ⁹ K. A. Matveev, Phys. Rev. B **70**, 245319 (2004).
 - ¹⁰ M. Casula, S. Sorella, and G. Senatore, Phys. Rev. B **74**, 245427 (2006).
 - ¹¹ L. Shulenburger, M. Casula, G. Senatore, and R. M. Martin, Phys. Rev. B **78**, 165303 (2008).
 - ¹² A. D. Güçlü, C. J. Umrigar, H. Jiang, and H. U. Baranger, Phys. Rev. B, **80**, 201302R (2009).
 - ¹³ A. C. Mehta, C. J. Umrigar, J. S. Meyer, H. U. Baranger Phys. Rev. Lett. **110**, 246802 (2013).
 - ¹⁴ S. V. Kravchenko and M. P. Sarachik, Rep. Prog. Phys. **67**, 1 (2004).
 - ¹⁵ H. Steinberg, O. M. Auslaender, A. Yacoby, J. Qian, G. A. Fiete, Y. Tserkovnyak, B. I. Halperin, K. W. Baldwin, L. N. Pfeiffer, and K. W. West, Phys. Rev. B **73**, 113307 (2006).
 - ¹⁶ O. M. Auslaender, A. Yacoby, R. de Picciotto, K. W. Baldwin, L. N. Pfeiffer, and K. W. West, Science **295**, 825 (2002).
 - ¹⁷ O. M. Auslaender, H. Steinberg, A. Yacoby, Y. Tserkovnyak, B. I. Halperin, K. W. Baldwin, L. N. Pfeiffer, and K. W. West, Science **308**, 88 (2005).
 - ¹⁸ V. V. Deshpande and M. Bockrath, Nature Physics **4**, 314 (2008).
 - ¹⁹ B. Brun, F. Martins, S. Faniel, B. Hackens, G. Bachelier, A. Cavanna, C. Ulysse, A. Ouerghi, U. Gennser, D. Mailly, S. Huant, V. Bayot, M. Sanquer, and H. Sellier, Nature Comm. **5**, 4290 (2014).
 - ²⁰ P. R. Wallace, Phys. Rev. **71**, 622 (1947).
 - ²¹ A. H. C. Neto, F. Guinea, N. M. R. Peres, K. S. Novoselov, and A. K. Geim, Rev. of Mod. Phys., **81**, 109 (2009).
 - ²² K. S. Novoselov, A. K. Geim, S. V. Morozov, D. Jiang, Y. Zhang, S. V. Dubonos, I. V. Grigorieva, A. A. Firsov, Science, **306**, 666 (2004).
 - ²³ Y. B. Zhang, Y. W. Tan, H. L. Stormer, P. Kim, Nature, **438**, 201 (2005).
 - ²⁴ C.-H. Zhang and Yogesh N. Joglekar, Phys. Rev. B, **75**, 245414 (2007).
 - ²⁵ R. Ct, J.-F. Jobidon, and H. A. Fertig Phys. Rev. B, **78**, 085309 (2008).
 - ²⁶ Hao Wang and V. W. Scarola Phys. Rev. B **85**, 075438 (2012).
 - ²⁷ K. A. Guerrero-Becerra, Massimo Rontani, Phys. Rev. B, **90**, 125446 (2014).
 - ²⁸ A. D. Güçlü, P. Potasz, M. Korkusinski, and P. Hawrylak, Graphene Quantum Dots Springer, Berlin, Heidelberg (2014).
 - ²⁹ K. Wakabayashi, M. Sigrist, and M. Fujita, J. Phys. Soc. Jpn. **67**, 2089 (1998).
 - ³⁰ Y.-W. Son, M. L. Cohen, S. G. Louie, Nature **444**, 347-349 (2006).
 - ³¹ O. V. Yazyev, M. I. Katsnelson, Phys. Rev. Lett. **100**, 047209 (2008).

- ³² B. Wunsch, T. Stauber, F. Sols, F. Guinea, Phys. Rev. Lett. **101** 036803 (2008).
- ³³ J. Jung and A. H. MacDonald, Phys. Rev. B **79**, 235433 (2009).
- ³⁴ M. Wimmer, I. Adagideli, S. Berber, D. Tomanek, and K. Richter, Phys. Rev. Lett. **100**, 177207 (2008).
- ³⁵ O. V. Yazyev, R. B. Capaz, and S. G. Louie, Phys. Rev. B **84**, 115406 (2011).
- ³⁶ A.D. Güçlü, M. Grabowski, P. Hawrylak, Phys. Rev. B **87**, 035435 (2013).
- ³⁷ M. Ezawa, Phys. Rev. B **76**, 245415 (2007).
- ³⁸ J. Fernandez-Rossier and J. J. Palacios, Phys. Rev. Lett. **99**, 177204 (2007).
- ³⁹ W. L. Wang, S. Meng, and E. Kaxiras, Nano Lett. **8**, 241 (2008).
- ⁴⁰ A. D. Güçlü, P. Potasz, O. Voznyy, M. Korkusinski, P. Hawrylak, Phys. Rev. Lett. **103**, 246805 (2009).
- ⁴¹ P. Potasz, A. D. Güçlü, A. Wojs, and P. Hawrylak, Phys. Rev. B **85**, 075431 (2012).
- ⁴² G. Z. Magda, X. Jin, I. Hagymasi, P. Vancso, Z. Osvath, P. Nemes-Incze, C. Hwang, L. P. Biro, L. Tapasztó. Nature **514**, 608 (2014).
- ⁴³ E. H. Lieb, Phys. Rev. Lett. **62**, 1201 (1989).